Journal of Power Sources 195 (2010) 6854–6859

Contents lists available at ScienceDirect

Journal of Power Sources

journal homepage: www.elsevier.com/locate/jpowsour

A novel sol–gel synthesis route to $NaVPO_4F$ as cathode material for hybrid lithium ion batteries

Jianqing Zhao, Jianping He*, Xiaochun Ding, Jianhua Zhou, Yi'ou Ma, Shichao Wu, Ruiming Huang

College of Material Science and Technology, Nanjing University of Aeronautics and Astronautics, Yudao Street 29, Nanjing, Jiangsu 210016, PR China

ARTICLE INFO

Article history:
Received 30 October 2009
Received in revised form 4 April 2010
Accepted 5 April 2010
Available online 10 April 2010

Keywords:
Hybrid lithium ion battery
Cathode material
Sol–gel method
$NaVPO_4F$

ABSTRACT

Sodium vanadium fluorophosphate, $NaVPO_4F$, a cathode material for hybrid lithium ion batteries has been synthesized via a modified sol–gel method followed by heat treatment. The vanadium (III) gel precursor as the reaction intermediate phase can be facilely prepared in ethanol under ambient conditions, and this synthesis considerably simplifies the conventional high-temperature fabrication of VPO_4. X-ray diffraction (XRD) results indicate a phase transition of $NaVPO_4F$ from the monoclinic crystal to the tetragonal symmetry structure. Meanwhile, the scanning electron microscope (SEM) images show the obvious spatial rearrangements on the morphology of samples. The hybrid lithium ion batteries based on the tetragonal $NaVPO_4F$ exhibit an even discharge plateau at 3.6 V vs. Li in the limited voltage range of 3.0–4.2 V, and the discharge capacity retention is up to 98.7% after 100 cycles at C/4 rate. With voltage excursion to 3.0–4.5 V, the initial charge and discharge deliver the reversible storage capacity of 117.3 and 106.8 mAh g^{-1}, respectively. Furthermore, the prepared $NaVPO_4F$ has a capacity retention of 83% after 100th cycle at 2 C rate. The electrochemical properties reveal the reversible mixed alkali ion (Li^+, Na^+) insertion reactions for this fluorophosphate material.

1. Introduction

Technological improvements in rechargeable lithium ion batteries have long been boosted by an ever-growing demand for high-end electronic devices, e.g., cellular phones, notebook computers and hybrid electronic vehicles. Currently commercial lithium ion batteries based on conventional transition metal oxide cathode materials, such as $LiCoO_2$ and spinel $LiMn_2O_4$, have been seriously prevented from extensive practical applications due to the underlying structural drawbacks [1]. In recent investigations, the polyanion phosphate and fluorophosphate materials including $LiFePO_4$ [2,3], $Li_3V_2(PO_4)_3$ [4,5] and $LiVPO_4F$ [6–8] have been proposed elsewhere because of the inherent thermal stability as safe alternatives for the traditional oxide cathodes. Among them, the presence of stable phosphate–metal bonds significantly decreases the probability of oxygen liberation from the structure [9]. Moreover, the inductive effect derived from phosphate-based functional groups enhances the working potential in comparison to the corresponding oxide [4]. Arroyo y de Dompablo et al. [10] theoretically investigated the positive effect of fluorine substitution on the electrochemical properties between the phosphate phase and the related fluorinated-polyanionic compounds. The computational results indicated that the introduction of fluorine into the phosphate-based structure increased the Li insertion voltage.

On the other hand, in addition to the safety concerns with the practical utilizations of lithium ion batteries, the cost of raw materials should also be taken into account to meet the rapidly commercial demand [11]. Therefore, it is essential to seek for other cheaper lithium-based alternatives. Considering the feasibility previously suggested by Barker et al. [12,13], the hybrid-ion approach adopted in existing lithium ion battery configuration has opened up a wider research region to many new sodium-based active cathode materials. The sodium vanadium fluorophosphates, involving $Na_3V_2(PO_4)_2F_3$ [9,11–13], $NaVPO_4F$ [14] and $Na_{1.5}VOPO_4F_{0.5}$ [15], have attracted considerable interest due to the far lower-cost raw materials, safer applications and higher working potential.

The $NaVPO_4F$ first proposed by Barker et al. [16] possesses a tetragonal symmetry structure (space group *I*4/*mmm*). The crystal structure is consistent with the sodium aluminum fluorophosphate (α-$Na_3Al_2(PO_4)_2F_3$), which was put forward by Meins et al. [17,18]. The related aluminum compound consists of a tridimensional framework built up from [$Al_2O_8F_3$] bioctahedra and [PO_4] tetrahedra. Wherein, the bioctahedra are composed of two [AlO_4F_2] octahedra bridged through an F vertex, and connect to each other through the [PO_4] tetrahedra by corner-sharing O vertex. This spatial arrangement generates cavities for the statistical distribution of sodium ions. The outstanding electrochemical properties of $NaVPO_4F$ have been demonstrated both in sodium ion [16] and

* Corresponding author. Tel.: +86 25 52112900; fax: +86 25 52112626.
E-mail address: jianph@nuaa.edu.cn (J. He).

0378-7753/$ – see front matter © 2010 Elsevier B.V. All rights reserved.
doi:10.1016/j.jpowsour.2010.04.003

hybrid lithium ion batteries [14]. The reversible alkali ion extraction/insertion performance is carried out based on the V^{3+}/V^{4+} redox couple. Zhuo et al. [19] have reported another interesting $NaVPO_4F$ phase, a monoclinic crystal with a space group of $C2/c$, which is in good agreement with the related $Na_3Al_2(PO_4)_2F_2$. This asymmetrical fabric is made up of two $[PO_4]$ tetrahedra that share two corner-oxygen atoms with two different $[VO_4F_2]$ octahedra. The sodium ions are statistically positioned in the tri-dimensionally spatial channels. Then, they investigated the advantageous effect of Cr-doping on the structural stabilization and the electrochemical cycle performance for $NaV_{1-x}Cr_xPO_4F$. The Cr-doped material had the better capacity retention than that of the un-doped. In our previous work [20], the improvements of C-doping on electrochemical characteristics of $NaVPO_4F$ were studied in lithium-based system, indicating that the 10 wt.% C-doped $NaVPO_4F$ showed a discharge capacity as high as 113 mAh g^{-1} at first cycle, and retained 91.6% of the original capacity after 20 cycles using a current density of 0.1 C rate.

In general, the sodium vanadium fluorophosphate materials have been conventionally synthesized by the two-process solid-state reaction or hydrothermal approach. The traditional synthesis requires VPO_4 as the reaction intermediate phase [9,12–16,19,20]. However, the prefabrication of VPO_4 in the solid-state reaction generally needs a complex operation procedure, high heating temperature and long time-consuming process. Likewise, in the hydrothermal route, there exists potential safety hazards caused by the generated very high pressure; besides, it is very complicated to collect resultant composites in post-procedures. Moreover, the low crystallinity of products may lead to unfavorable degradation of electrochemical properties [14]. Therefore, lots of research work should be undertaken to optimize the synthetic methodology and enhance the electrochemical performance. To the best of our knowledge, there has been little study on sol–gel synthesis of fluorophosphates [7,11], particularly for $NaVPO_4F$. In this paper, we adopted a novel sol–gel strategy followed by heat treatment to prepare $NaVPO_4F$, and its electrochemical performance was evaluated in lithium-based cell configuration. The hybrid lithium ion batteries have exhibited remarkable charge/discharge reversibility, satisfied cycle performance and outstanding high-rate characteristics.

2. Experimental

2.1. Synthesis of $NaVPO_4F$ by a sol–gel method

In this facile run, the reactants of V_2O_5 and oxalic acid (molar ratio = 1:6) were dissolved in ethanol, and then strongly stirred at constant 80 °C until the orange reactive solution turned to fresh green. Stoichiometric $NH_4H_2PO_4$ and NaF were added with continuous agitation. Green sol mixture was formed by adjusting the pH with ammonia. The moist sol compound was transferred to heat at 80 °C in a vacuum oven for 24 h. And then, the dried gel precursor was ground and sintered in a tube furnace under flowing nitrogen for 6 h. In order to investigate the optimal heating temperature, three candidate temperatures (700 °C, 750 °C and 800 °C) were chosen from the thermal analyses to sinter the gel-stated samples, respectively.

2.2. Characterization of composites

Characteristic weight loss and thermodynamic heat energy transmission of gel precursor were estimated from thermogravimetric (TG)/differential scanning calorimetric (DSC) analyses using a New Castle TA Q10 thermoanalyzer. The measurement was performed at a scan rate of 5 °C min^{-1} with a temperature range from room temperature to 900 °C in nitrogen atmosphere. The crystallographic structure and phase were determined by X-ray powder diffraction (XRD) utilizing a Bruker D8 X-ray diffraction meter with monochromatic Cu Kα radiation. The particle size and surface morphology of the samples were observed by a FEI Quanta 200 scanning electron microscopy (SEM).

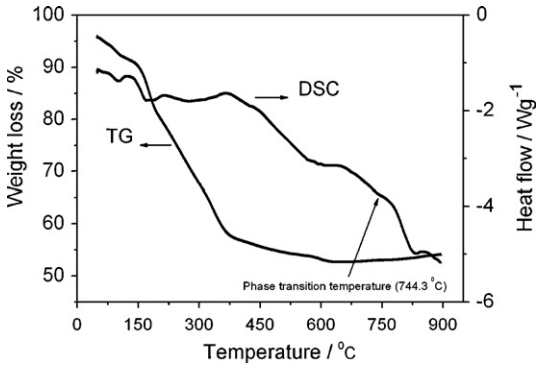

Fig. 1. Thermal analysis patterns of the gel precursor between room temperature and 900 °C at a scan rate of 5 °C per minute in nitrogen atmosphere.

2.3. Electrochemical measurements

The cathode electrode mixtures comprised 75 wt.% of active material, 15 wt.% of acetylene black (conductive carbon) and 10 wt.% of polyvinylidenefluoride (PVDF) binder, dissolved in 1-methyl-2-pyrrolidone (NMP). The black viscous slurry was plastered onto the aluminum foil as the current collector and dried at 130 °C under vacuum for 24 h. The circular electrode in a diameter of 16 mm was loaded ~3 mg of active material. The homemade testing cells were assembled in an argon-filled glove box including the prepared cathode electrode, metallic lithium as the anode electrode and Celgard-2400 membrane as the separator. The electrolyte was 1 M $LiPF_6$ dissolved in ethylene carbonate (EC) and dimethyl carbonate (DMC) with the volumetric ratio of 1:1. The electrochemical properties of $NaVPO_4F$ as cathode material were evaluated in the typical lithium ion battery configuration. Galvanostatic charge/discharge reactions and cyclic voltammetry (CV) tests were carried out in the voltage cut-offs of 3.0–4.2 and 3.0–4.5 V using the CT2001A LAND battery tester and the electrochemical workstation (CHI660C), respectively. The electrochemical storage capacity of sample was calculated on the mass of active material, and the CV characterization was performed at a scan rate of 0.1 mV s^{-1}.

3. Results and discussion

Sodium vanadium fluorophosphates have been conventionally synthesized using the two-step solid state or hydrothermal method. The reaction intermediate phase is the orthorhombic vanadium (Ш) phosphate (VPO_4), prefabricated by the high-temperature carbothermal reduction reaction. In this paper, we exploited a novel sol–gel method to introduce a facile synthesis of the vanadium (Ш) intermediate phase in the ethanol solution. The color of reactive solution changes from orange (V^{5+}) to blue (V^{4+}), and the ultimate stability of green (V^{3+}) obviously signifies the formation of vanadium (Ш) precursor. The $NaVPO_4F$ can be obtained by sintering uniform sol–gel mixtures. This modified approach remarkably simplifies the experimental procedure to effectively take advantage of reactive energy and is time saving.

The TG/DSC curves are shown in Fig. 1 in order to determine the most suitable sintering temperature for the gel precursor. The slight weight loss from TG curve appears around 102 °C due to the volatilization of residual water and organic solvents. The total

mass declines abruptly to 53% when the gel precursor is undergone to fire from 124 °C to 613 °C. This mass loss is probably assigned to the decomposition of $NH_4H_2PO_4$ and the pyrolysis of organic compounds [11]. The weight of testing mixtures hardly decreases above 700 °C. In contrast, two well-resolved peaks indicative of the heat flow transformation are detected in DSC profile up to 835 °C along with a visible turning point at near 750 °C. The distinct phenomenon presumably results from a phase transition when the composites are subjected to the gradually increased heating process. Therefore, three sintering temperatures (700 °C, 750 °C and 800 °C) were chosen to prepare the target samples, and the resultant products were labeled as T700, T750 and T800, respectively.

Fig. 2 displays the XRD patterns of three samples. The pattern for T700 (Fig. 2a) suggests the phase of monoclinic crystal (space group $C2/c$). The lattice parameters of crystal cell are generated: $a = 1.273$ nm, $b = 0.637$ nm, $c = 0.897$ nm, $\alpha = \gamma = 90.00°$, $\beta = 102.31°$. These results are in good agreement with that reported by Zhuo et al. [19]. As the sintering temperature approaching 750 °C, the dominant phase of T750 in Fig. 2b is a tetragonal symmetry structure (space group $I4/mmm$) with the following crystallographic parameters: $a = b = 0.638$ nm, $c = 1.072$ nm, $\alpha = \beta = \gamma = 90.00°$. The position and intensity of the diffraction peaks agree well with the previous work published by Barker et al. [14,16]. Hence, the XRD results confirm that the pre-hypothetic phase transition happens in terms of the above-mentioned DSC analysis. When the temperature is up to 800 °C, as shown in Fig. 2c, the ultimate compounds are amorphous, and the $NaVPO_4F$ phase is non-observable. However, the diffraction peaks characteristic of karelianite (V_2O_3), vanadium phosphide (V_2P) and vanadium phosphate of $V_4(P_4O_{12})_3$ are detected. It is reasonable that the amorphous mixtures should come from the decomposition of the fluorophosphate material, which results in the loss of light elements (Na and F) as well as the collapse and reconstruction of phosphate groups [15].

The significant effect of heat treatment on the morphology of samples can be estimated from SEM images (Fig. 3). The obvious spatial rearrangements of three samples have been made by the gradually increased calcinations. In Fig. 3a, the granular T700 aggregates tightly to construct an interconnecting layered structure. As for T750, the separate shapeless particles are observed with the micrometric size of 5–10 μm (Fig. 3b), which is medium-sized among the analogues prepared by the solid state and the hydrothermal method [14]. In addition, large quantities of visible macropores are created throughout the whole product (Fig. 3b). The increased heating temperature facilitates the degradation of the organic groups and promotes the gas release, so as to generate this porous framework architecture [21]. Generally speaking, the porous fabric of the active material is favorable for the permeability of the electrolyte into the internal structure, and shortens the pathway of lithium ion diffusion. The porosity therefore considerably contributes to the improvement of electrochemical performance. Interestingly in Fig. 3c, the spongy-shaped compound is shown in porous network. As demonstrated by XRD result (Fig. 2c), the breakage of $NaVPO_4F$ gives rise to this formation of glass ceramic phase when the temperature goes beyond 800 °C.

The electrochemical properties of three samples (T700, T750 and T800) as cathode materials were preliminarily tested in lithium-based electrolyte phase with metallic lithium as anode. Fig. 4 illustrates the curves of voltage vs. capacity for the first

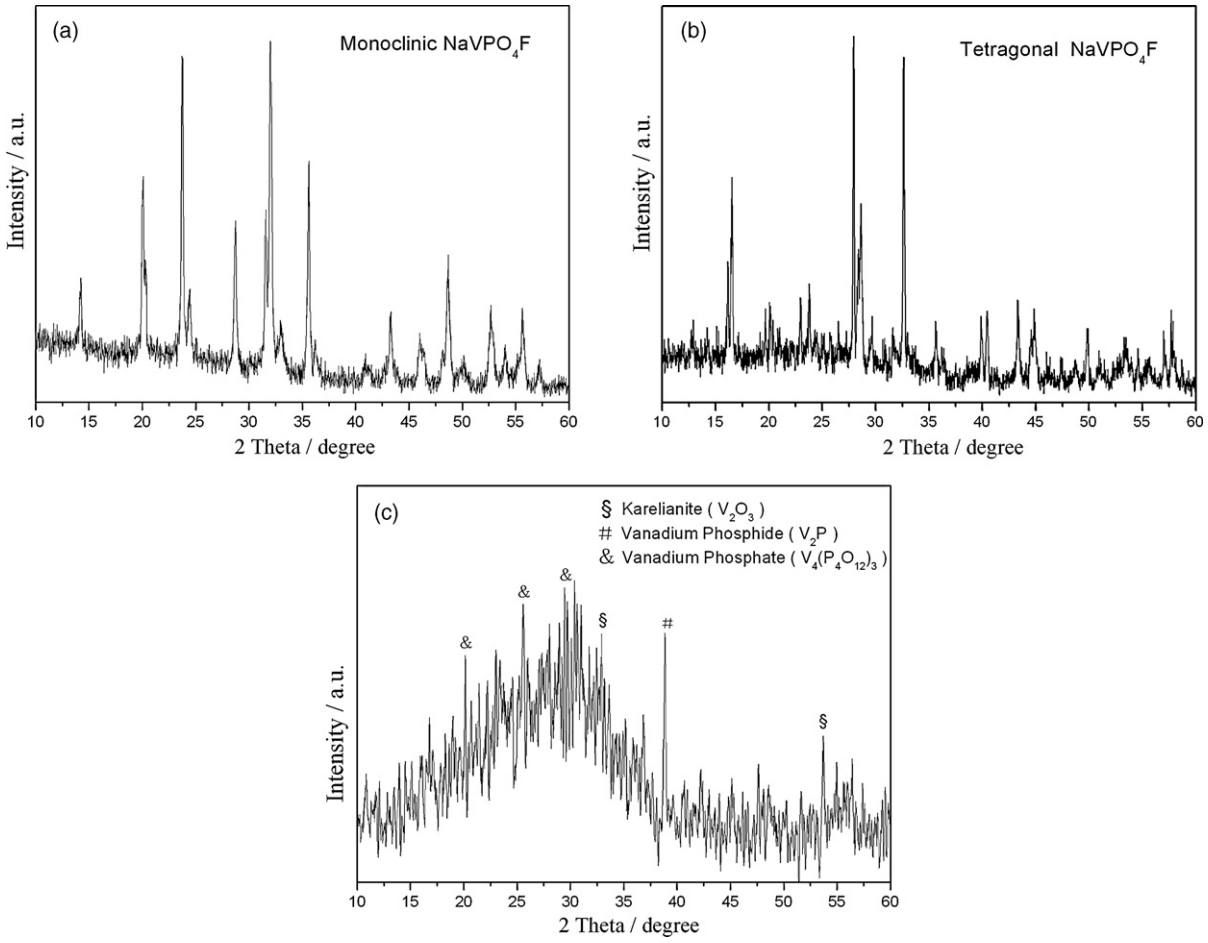

Fig. 2. XRD patterns of three samples. (a) T700, (b) T750 and (c) T800.

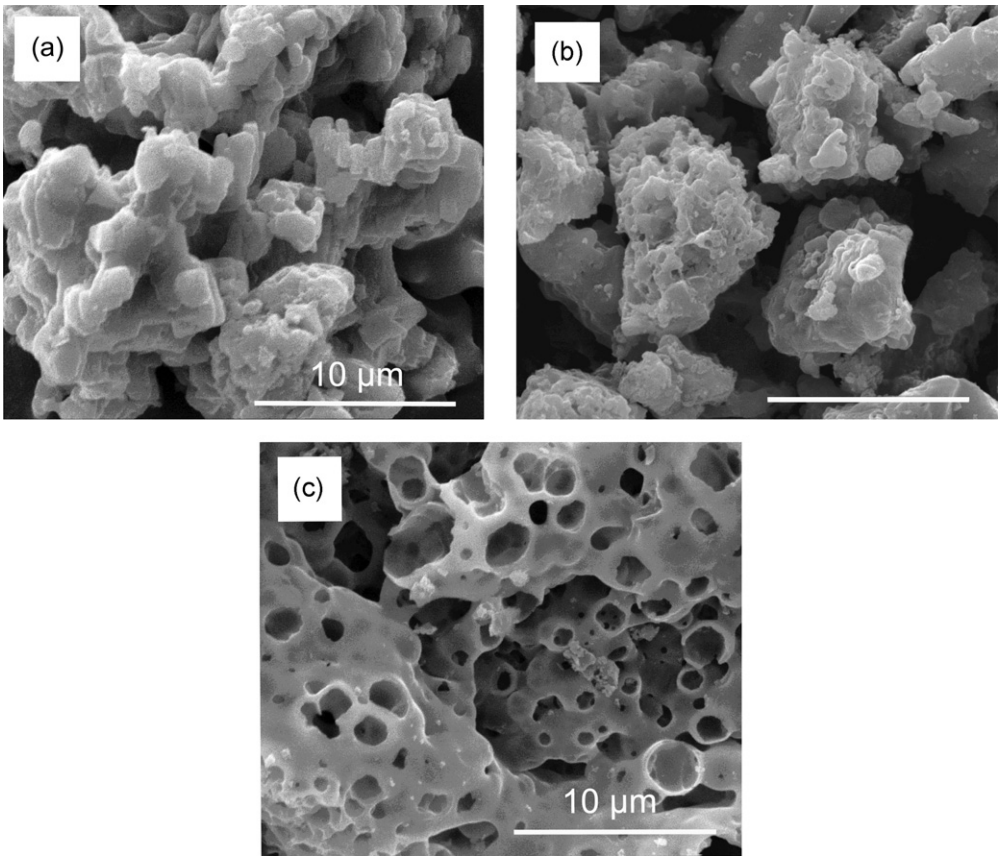

Fig. 3. SEM micrographs of three samples. (a) T700, (b) T750 and (c) T800.

charge/discharge reactions in the voltage range between 3.0 and 4.2 V. By comparison with the electrochemical behaviors, T750 exhibits the superior storage capacity and reversible intercalation, which are mainly attributed to its tetragonal symmetry structure and porous fabric. Therefore, the advanced investigations of T750 as positive electrode were carried out in hybrid lithium ion batteries as follows: the cut-off voltage was chosen according to the current lithium ion cell configuration [1] and the work of Barker et al. [14]. The charge–discharge performance and CV measurements were performed between 3.0–4.2 and 3.0–4.5 V, respectively, in order to remove the equivalent of 0.5 and 1 lithiums. All assembled cells were tested immediately in order to reduce the likelihood of appreciable ion exchange between $NaVPO_4F$ and the Li^+-based electrolyte [11–14]. The mechanism interpretation of alkali ion intercalation and deintercalation in Na-based cathode materials, such as $Na_3V_2(PO_4)_2F_3$ [11–13] and $NaVPO_4F$ [14], has been firstly proposed by Barker et al. [12–14], and recently demonstrated by Wei and co-workers [11]. During the initial charge process, sodium ions extract from the $NaVPO_4F$, and then enter into the electrolyte to form a binary Li^+/Na^+ electrolyte. On the subsequent discharge, the Li^+ ions replace the partial Na^+ ions at the same crystallographic sites in the fluorophosphate framework. In other words, a simultaneous insertion reaction of Li^+ and Na^+ occurs. Finally, the electrochemical insertion of $NaVPO_4F$ in hybrid lithium ion battery shifts gradually from a predominant Na^+ insertion to a Li^+ insertion in cycles [11].

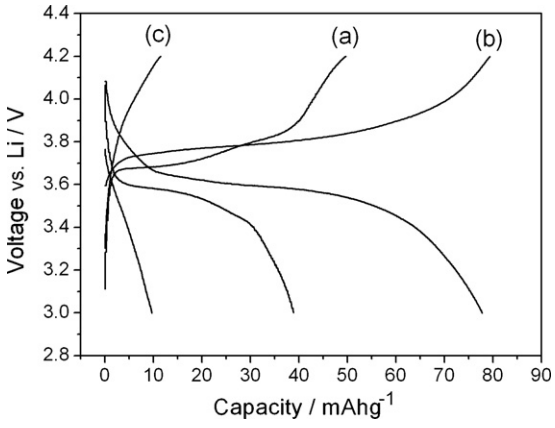

Fig. 4. First charge/discharge curves of three samples vs. Li at a current density of C/4 between 3.0 and 4.2 V. (a) T700, (b) T750 and (c) T800.

Fig. 5 shows the charge and discharge curves in the limited voltage range between 3.0 and 4.2 V, which is well compatible with the voltage cut-off in the current commercial lithium ion batteries. The $NaVPO_4F$ delivers a charge capacity of 79.4 mAh g^{-1} under the current density of C/4, equivalently converted to $x = 0.55$ in $Na_{1-x}VPO_4F$ (the theoretical capacity is 143 mAh g^{-1}). The corresponding discharge capacity is 76.7 mAh g^{-1}, indicating a high initial coulombic efficiency of 96.6%. It also reveals an even discharge plateau around 3.6 V vs. Li. The cell retains 98.7% of the original discharge capacity at the 100th cycle, denotative of a relatively low capacity fade behavior. In addition, there are perceptible changes in charge/discharge curves between 5th and 25th cycle and slight differences after that. This transformation in electrochemical performance presumably reveals that the Li^+ insertion has substituted for the Na^+ insertion to dominate the electrochemical insertion of $NaVPO_4F$ after the 25th cycle. Furthermore, Fig. 6 compares the CV characterization of the pristine assembled cell with that replayed after 100 charge/discharge cycles. As the debut shown, a well-defined couple of redox peaks locates at 3.84

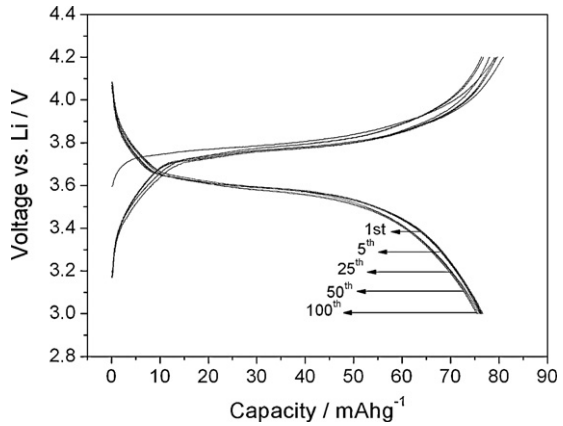

Fig. 5. Galvanostatic charge/discharge performance of the tetragonal $NaVPO_4F$ vs. Li at C/4 rate in the limited voltage range of 3.0–4.2 V in hybrid lithium ion battery.

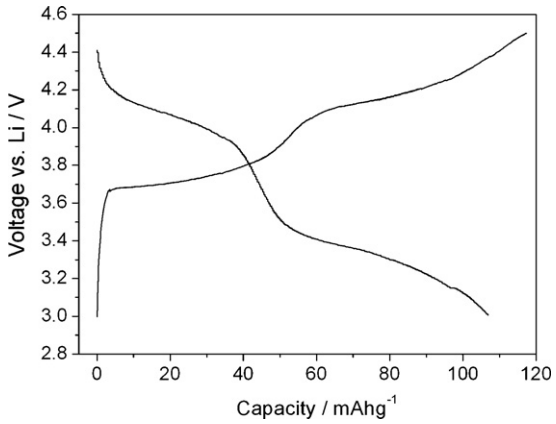

Fig. 7. First charge/discharge curves of the tetragonal $NaVPO_4F$ vs. Li at C/4 rate in the voltage range of 3.0–4.5 V in hybrid lithium ion battery.

and 3.62 V in consistence with the result of the first galvanostatic charge/discharge curves (Fig. 5). Both the low-level voltage hysteresis in CV figure and the generally symmetrical nature of the charge/discharge profile imply the dominant Na^+ reinsertion reaction and express the favorable energetic reversibility of the sodium ion intercalation. Somewhat enhanced polarization was recorded in the re-acted CV pattern on the 100 times cycled cell, which should be caused by the transformation of insertion mechanism from a predominant Na^+ insertion to a Li^+ insertion. However, the small voltage gap still remains between 3.87 and 3.59 V in good agreement with the figure of 100th cycle curves (Fig. 5). Therefore, the electrochemical properties indicate the structural rigidity and reversible mixed alkali ion (Li^+, Na^+) insertion reactions in this fluorophosphate material. Overall, the favorable electrochemical performance of $NaVPO_4F$ can be suitable for the current lithium ion cell infrastructure and well comparable with the practical applications in this limited voltage range.

The initial cycle of $NaVPO_4F$ in the extended voltage cut-off of 3.0–4.5 V is obtained in Fig. 7. At the same current density of C/4, the dual voltage plateaus are observed both in the charge and discharge curves, respectively. In the initial charge, the two-step extraction of sodium ions from the host fluorophosphate framework is confirmed by the double voltage plateaus positioned at 3.7 and 4.2 V, and the equivalent reinsertion of alkali ions happens at 4.1 and 3.4 V in the subsequent discharge reaction. The total charge capacity is 117.3 mAh g^{-1}, which amounts to $x = 0.82$ in $Na_{1-x}VPO_4F$ (the theoretic capacity is 143 mAh g^{-1}). Correspondingly, the discharge capacity is 106.8 mAh g^{-1}, converting to the coulombic efficiency of 91.0%. The double voltage plateaus reveal that sodium ions in the tetragonal symmetric $NaVPO_4F$ structure occupy two non-equivalent crystallographic sites [16] and can intercalate and deintercalate step by step through the active cathode material under the wider voltage cut-off with the upper voltage up to 4.5 V. Therefore, it is not surprising that the dual voltage plateaus disappear as shown in Fig. 5 when the upper voltage in cut-off decreases to 4.2 V or under the narrower voltage range. The approximate symmetry of the first charge/discharge curves again proves the predominant Na^+ insertion mechanism in the successive discharge reaction. The cycle performance and rate characteristics of the $NaVPO_4F$ were tested in these hybrid lithium ion batteries, and the results are shown in Fig. 8. The $NaVPO_4F$ has the initial discharge capacity of 106.8 mAh g^{-1} and declines by about 10% of storage capacity to 96.0 mAh g^{-1} after 100 cycles at C/4 rate. The satisfied retention, as high as 83%, is obtained even at the 2 C rate. Complementarily, the mixed Li^+/Na^+ insertion reactions do not lead to unfavorable influence on the long-term cycling stability. The almost parallel figures in Fig. 8 shows a desirable tendency of discharge capacity retention and denotes outstanding rate characteristics of the fluorophosphate sample. However, a higher capacity fade occurs at the initial cycles, which is similar to the results reported by Barker et al. [14]. Two proposed reasons might interpret the capacity loss at the beginning period: (1) in hybrid lithium-based testing system, mixed alkali ions reinsert into and replace Na^+ sites in the structure after the first charge

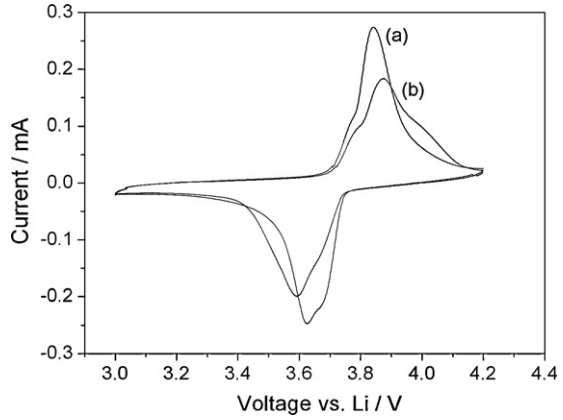

Fig. 6. CV characterization recorded for the tetragonal $NaVPO_4F$ vs. Li at a scan rate of 0.1 mV s^{-1} in the limited voltage range of 3.0–4.2 V. (a) The pristine assembled cell, (b) re-acted after 100 charge/discharge cycles.

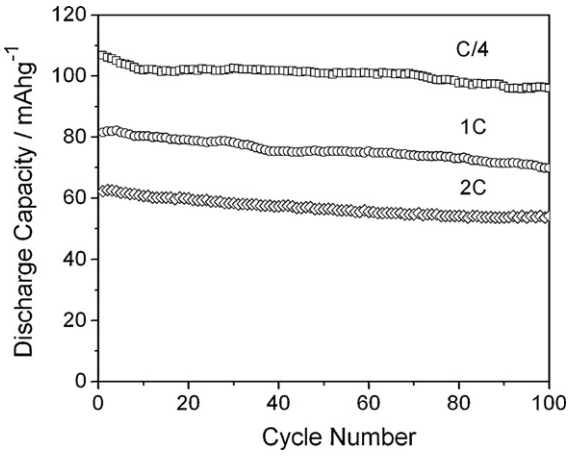

Fig. 8. Cycle performance and rate characteristics of the tetragonal $NaVPO_4F$ vs. Li in the voltage range of 3.0–4.5 V in hybrid lithium ion batteries.

reaction. Because of the smaller size of Li^+ compared to Na^+, the replacement may cause phase transformation or volume contraction to block the insertion of alkali ions until a new stable structure is reconstructed; (2) the vanadium-based polyanion materials are extremely easy to dissolve in $LiPF_6$-based electrolyte [14], which should take responsibility for the perceptible capacity reduction. In our experiments, a slight discoloration of light green can be seen on the separator membrane, corresponding to the vanadium dissolution. In conclusion, considering the overall cycle performance in long trials, the hybrid lithium ion batteries exhibit favorable storage capacity, insertion stability and high-rate characteristics. The $NaVPO_4F$ prepared by sol–gel method can be available as cathode material in lithium ion batteries for the practical applications.

4. Conclusions

In this paper, a novel sol–gel approach was developed to synthesize the tetragonal $NaVPO_4F$ (space group $I4/mmm$). On the basis of TG/DSC, XRD and SEM analyses, we demonstrated the phase transition of $NaVPO_4F$ gradually from the monoclinic crystal at 700 °C to the tetragonal structure at 750 °C, and final decomposition when the heating temperature went beyond 800 °C. The obvious changes on morphology of samples were observed from the micrographs. The tetragonal $NaVPO_4F$ provides two non-equivalent crystallographic sites for accommodating sodium ions in the host fluorophosphate framework. In the limited voltage range of 3.0–4.2 V, the hybrid lithium ion batteries based on the tetragonal $NaVPO_4F$ as cathode material exhibit an average discharge voltage around 3.6 V vs. Li and the excellent discharge capacity retention more than 98.7% at the 100th cycle at low rates. When the voltage cut-off extends to 3.0–4.5 V, the initial charge reaction delivers a specific capacity of 117.3 mAh g^{-1} with the dual voltage plateaus at the C/4 rate, which equivalently converts to $x = 0.82$ in $Na_{1-x}VPO_4F$ (the theoretic capacity is 143 mAh g^{-1}). The $NaVPO_4F$ also shows outstanding rate characteristics and structural stability in contribution to 83% of capacity retention after 100 cycles at the high current density of 2 C. In light of the remarkable electrochemical properties together with low cost, safety and simple synthesis, the sol–gel synthesized $NaVPO_4F$ is a promising cathode candidate in hybrid lithium ion batteries.

Acknowledgments

The authors appreciate the financial support of the National Natural Science Foundation (50871053) and Aeronautical Science Foundation of China (2007ZF52061).

References

[1] J.-M. Tarascon, M. Armand, Nature 414 (2001) 359–367.
[2] A.K. Padhi, K.S. Nanjundaswamy, J.B. Goodenough, J. Electrochem. Soc. 144 (1997) 1188–1194.
[3] B. Kang, G. Ceder, Nature 458 (2009) 190–193.
[4] Y. Li, Z. Zhou, M. Ren, X. Gao, J. Yan, Electrochim. Acta 51 (2006) 6498–6502.
[5] P. Fu, Y. Zhao, Y. Dong, X. An, G. Shen, Electrochim. Acta 52 (2006) 1003–1008.
[6] J. Barker, R.K.B. Gover, P. Burns, A. Bryan, M.Y. Saidi, J.L. Swoyer, J. Power Sources 146 (2005) 516–520.
[7] Y. Li, Z. Zhou, X.P. Gao, J. Yan, J. Power Sources 160 (2006) 633–637.
[8] R.K.B. Gover, P. Burns, A. Bryan, M.Y. Saidi, J.L. Swoyer, J. Barker, Solid State Ionics 177 (2006) 2635–2638.
[9] R.K.B. Gover, A. Bryan, P. Burns, J. Barker, Solid State Ionics 177 (2006) 1495–1500.
[10] M.E. Arroyo y de Dompablo, U. Amador, J.-M. Tarascon, J. Power Sources 174 (2007) 1251–1257.
[11] T. Jiang, G. Chen, A. Li, C. Wang, Y. Wei, J. Alloys Compd. 478 (2009) 604–607.
[12] J. Barker, R.K.B. Gover, P. Burns, A.J. Bryan, Electrochem. Solid State Lett. 9 (2006) A190–A192.
[13] J. Barker, R.K.B. Gover, P. Burns, A.J. Bryan, J. Electrochem. Soc. 154 (2007) A882–A887.
[14] J. Barker, M.Y. Saidi, J.L. Swoyer, J. Electrochem. Soc. 151 (2004) A1670–A1677.
[15] F. Sauvage, E. Quarez, J.-M. Tarascon, E. Baudrin, Solid State Sci. 8 (2006) 1215–1221.
[16] J. Barker, M.Y. Saidi, J.L. Swoyer, Electrochem. Solid State Lett. 6 (2003) A1–A4.
[17] J.-M. Le Meins, O. Bohnke, G. Courbion, Solid State Ionics 111 (1998) 67–75.
[18] J.-M. Le Meins, M.-P. Crosnier-Lopez, A. Hemon-Ribaud, G. Courbion, J. Solid State Chem. 148 (1999) 260–277.
[19] H. Zhuo, X. Wang, A. Tang, Z. Liu, S. Gamboa, P.J. Sebastian, J. Power Sources 160 (2006) 698–703.
[20] C.X. Zhang, J. He, G. Zhao, J. Zhao, Chin. J. Inorg. Chem. 23 (2007) 649–654.
[21] R. Dominko, M. Bele, J.-M. Goupil, M. Gaberscek, D. Hanzel, I. Arcon, J. Jamnik, Chem. Mater. 19 (2007) 2960–2969.